A comparison of the galling wear behaviour of PVD Cr and electroplated hard Cr thin films

J.L. Daure [a] [*]

jaimie.daure@nottingham.ac.uk

M.J. Carrington [a]

P.H. Shipway [a]

D.G. McCartney [a]

D.A. Stewart [b]

[a]Advance Materials Research Group, Faculty of Engineering, The University of Nottingham, University Park, Nottingham NG7 2RD, UK

[b]Rolls-Royce PLC, Raynesway, Derby DE21 7XX, UK

Abstract

Electroplated hard chromium (EPHC) is used in many industries as a wear and corrosion resistant coating. However, the long term viability of the electroplating process is at risk due to legislation regarding the toxic chemicals used. The physical vapour deposition (PVD) process has been shown to produce chromium and chromium-based coatings that could be a possible alternative for EPHC in some applications. This study investigates the microstructure and properties of two PVD chromium coatings as a possible alternative to EPHC to provide resistance to galling. Two PVD deposition processes are investigated, namely electron beam PVD (EBPVD) and unbalanced magnetron sputtering (UMS). Galling wear tests were performed according to ASTM G98-17. The results show that the two PVD coatings are of similar hardness, surface roughness and exhibit similar scratch behaviour. However, the galling wear resistance of the coating deposited by UMS is approximately ten times that of the EBPVD coating, and similar to that of the EPHC. X-ray diffraction reveals that the EBPVD chromium coating has a strong preferred orientation of the {2 0 0} planes parallel to the coating surface whilst in the UMS PVD coating, preferred orientations of the {1 1 0} and {2 1 1} planes parallel to the surface are observed. The EPHC does not exhibit relative peak intensities which conform to the International Centre for Diffraction Data (ICDD) powder diffraction pattern consistent with chromium. The crystal orientation of the PVD chromium coatings appears to play a significant role in influencing galling resistance.

1   Introduction

Electroplated chromium coatings are widely used in industry for both functional and decorative applications due to their excellent wear and corrosion resistance [1-4]. Electroplated hard chromium (EPHC) is used in many applications such as shock absorber rods, hydraulic cylinders, crankshafts, industrial rolls and many more [2]. However, the deposition of EPHC utilises hazardous hexavalent chromium baths. Due to the toxicity of Cr(VI) to workers and the environment, regulations (EU Regulation (EC) No 1907/2006 ("REACH") [5]) which forbid or severely limit the use of chromium trioxide baths mean that there is a need to seek replacements for EPHC in a range of applications [1-6]. In light of the above, research is being conducted into the use of dry coatings such as physical vapour deposition (PVD), chemical vapour deposition (CVD) and thermal spraying [7-10]. Some examples of alternative coatings that have been investigated are electrodeposited chromium from trivalent baths using $CrCl_3$ or $Cr_2(SO_4)_3$, high velocity oxy-fuel sprayed WC-Co and vapour deposited Cr, CrN, CrC, TiN and TiAlN [6, 7, 9, 11].

Among these alternatives, PVD has been reported to be one of the most promising coating methods for the replacement of coatings under 10 μm in thickness [7]. Two common PVD techniques are electron beam (EB) PVD and unbalanced magnetron sputtering (UMS) PVD. EBPVD utilises high-energy electron beams generated from electron guns to melt and evaporate the target, and exhibits high deposition rates and low contamination of deposits. In magnetron sputtering, atoms are physically ejected from the target by ion bombardment resulting in less heating of the substrate surface [12, 13].

In industrial applications, coatings are used to protect components against wear or corrosion in aggressive environments. PVD Cr and Cr-based coatings have been shown to

exhibit high sliding wear resistance in many applications [7, 14, 15]. For most metals, PVD coatings thicker than 3-5 μm can be problematic due to high internal stresses; however, this has been observed not to be the case for PVD Cr and Cr-based coatings which can be deposited with thicknesses up to 20 μm [7]. One of the limiting factors of PVD coatings is growth defects which can have a strong negative impact on the tribological properties of the coatings. High contact pressures at these raised defects can initiate cracking, develop abrasive particles and result in coating failure [16, 17]. Studies have shown that a polished coating which has been deposited on a polished substrate can reduce defect density and therefore enhance the tribological performance of PVD coatings; however, in industrial applications, it is generally not feasible or economic to polish a component following coating [16, 17].

One of the least well understood wear failure modes of materials and coatings in industry is galling. Galling is a form of adhesive wear which generally results in material transfer and material being raised from a surface which impedes sliding against other surfaces. This can often result in seizure of contacting components [18-20]. Whilst galling is still not comprehensively understood, research has been conducted into the effect of material hardness, composition, surface roughness, surface defects, lubrication and temperature on galling resistance [16, 18, 19, 21]. It is often reported that a higher hardness and a lower surface roughness increases the galling resistance of a tribological system [17-19, 21].

Examples of industries that suffer significantly from galling include sheet metal stamping and industries which cannot adequately lubricate sliding surfaces due to contamination problems (such as sanitary systems, food processing, medical devices, nuclear reactors etc.) [18-20, 22].

The current research focus in the field of electroplated chromium replacement is predominantly focussed on alternative coatings other than pure chromium. Little work has been conducted to date regarding the deposition of pure chromium by vapour deposition methods. This study aims to characterise PVD chromium, deposited by two commercially available methods, and compare the galling behaviour with conventional commercially-deposited EPHC. This will be done by characterising the as-deposited coatings and conducting an investigation of the failure mechanisms following galling wear testing using X-ray diffraction, optical and scanning electron microscopy

2 Experimental methods

2.1 Materials

Three chromium coatings, deposited onto grade 316 austenitic stainless steel substrates, were obtained from commercial suppliers. Prior to coating, the substrates were ground to an Ra of ~ 0.2 μm and cleaned in an ultrasonic bath of industrial methylated spirit before being dried in air. Two of the coatings were deposited by physical vapour deposition (PVD) and the other coating was deposited by conventional hard chrome electroplating (EPHC) to act as a baseline in the study. One of the PVD coatings was deposited by electron beam physical vapour deposition (EBPVD) to a thickness of 7.7 ± 0.4 μm whilst the other was deposited by unbalanced magnetron sputtering (UMS) to a thickness of 7.8 ± 0.2 μm. The hard chrome plating (EPHC) coating had a thickness of 9.6 ± 0.2 μm.

Grade 316 austenitic stainless steel was employed as the counterface in the galling wear tests.

2.2   Material Characterisation

X-Ray diffraction

X-ray diffraction (XRD) was performed on the as-received surfaces of coatings to identify the phases present. Scans over a 2θ range of 40 to 90 ⁰ were conducted using a Bruker D500 X-ray diffractometer with Cu K-alpha radiation of wavelength 0.15406 nm. The working voltage and current used were 40 kV and 25 mA respectively. XRD data were collected using a step size of 0.02° and a counting time per step of 2 seconds. Phases present were identified using the International Centre for Diffraction Data (ICDD) database.

Peak widths at half maximum were measured and used to estimate grain size using the Scherrer equation:

$$\tau = \frac{0.94\,\lambda}{\beta\,\cos\theta}$$

where τ is the average crystallite size, β is the line broadening, θ is the Bragg angle and λ is the X-ray wavelength [23]. Instrumental broadening was accounted for in the calculations by using a scan of lanthanum hexaboride and subtracting the relevant peak width from β.

Metallurgical sample preparation and microscopy

Metallographic cross-sections were prepared in a hot-mount conductive resin to ASTM E3-11. To remove any effects associated with cutting the specimen, following mounting, the surface to be viewed was ground back using a 220-grit SiC paper. Progressive grinding with finer grades was carried out, finishing with 1200-grit SiC paper, followed by automated polishing with successively finer diamond pastes (6 and 1 μm). To examine the damage to the coatings following testing, galling wear scars were sectioned chordally towards the outer limits of the scar (so that the plane of the section was parallel to the direction of shear in the centre of the scar) and prepared as per the metallographic cross-sections.

Scanning electron microscopy (SEM) was utilised to examine the as-received surfaces of coatings, polished cross-sections and sample surfaces following wear testing. Samples were examined by secondary electron (SE) and backscattered electron (BSE) imaging using a FEI XL 30 SEM operating at 20 kV.

Surface roughness

White light interferometry was used to measure the surface roughness of the as-received coatings. The analysis was carried out using a Bruker ContourGT-I 3D Optical Microscope and Vision64 software. Ra values of surface roughness were measured using a 20x objective lens. Four measurements were taken at different positions on the surface and a mean Ra value was obtained.

2.3 Mechanical testing

Nanoindentation

Coating hardness was determined using a Micro Materials Ltd Platform three instrument, with measurements being carried out in accordance with ISO 14577-4. Tests were conducted on the as-received top surface of coatings on 8 x 8 x 1 mm square sections using a diamond Berkovich indenter at a load of 100 mN, in order to stay within 10% of the film thickness, with a loading and unloading time of 20 s and a dwell period of 10 s at maximum load. Ten indentations were carried out on each sample to obtain a mean value and a standard deviation. The hardness was calculated using NanoTest Platform Three software from Micro Materials Ltd using the maximum applied load (P_{max}) and the residual indentation area (A_r), $H = \frac{P_{max}}{A_r}$. The area function of the indenter was calibrated using a material of known properties, in this case fused silica.

Scratch testing

Coating fracture resistance was determined by scratch testing as shown schematically in Figure 1. Tests were conducted in accordance with the ASTM C1624-05 standard, under unlubricated conditions in air and at room temperature. A Rockwell C diamond stylus was used on a multi-specimen tribo-test system from CETR.

Scratch tests were conducted between 0 and 90 N over a distance of 5 mm on the as-received coating surface. A loading time of 30 seconds was used, resulting in a sliding speed of 10 mm/min, and a continuous loading rate of 180 N/min.

Five scratches were conducted on each sample. The damage events along the scratch tracks were analysed using optical microscopy and SEM.
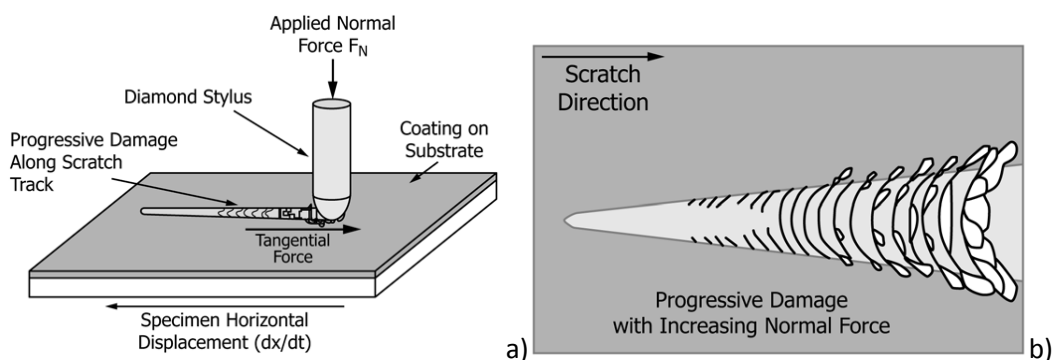

Figure 1 Schematic diagram of (a) scratch test (b) scratch scar [24]

Wear testing

Galling wear testing was carried out in accordance with ASTM G98-17 as shown schematically in Figure 2. Galling wear tests were performed by loading a flat faced austenitic stainless steel grade 316 (Ø12.7 mm) pin against a coated stainless steel 316 disc (Ø30 mm x 10 mm). The microhardness of the 316 was roughly 2.0 GPa. The galling tests were carried out using an Instron 5581 test machine with a 50 kN load cell. Once

loaded, one full revolution of the pin was carried out; the load was then removed, the pin taken from the rig and the surfaces of pin and disc inspected for initial evidence of material transfer or coating delamination in an optical microscope. If no evidence of material transfer was present, the test was repeated with a new pin and on an untested region of the coated surface at a higher contact pressure. Contact pressures were applied at 7, 15 and 25 MPa then incremented in steps of 25 MPa thereafter. Once galling had occurred, the contact pressure was lowered and the test repeated to find the lowest stress at which galling occurs. Wear scars were analysed using optical microscopy and SEM.
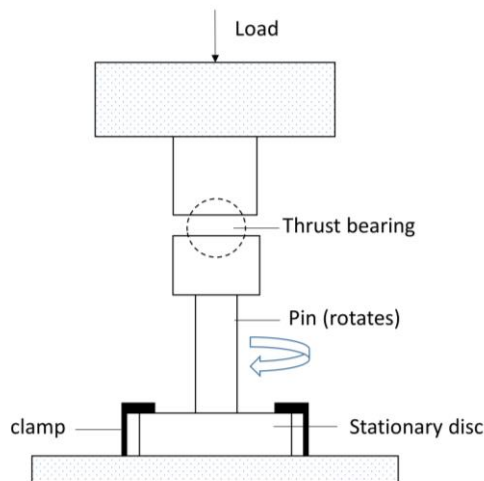

Figure 2 Schematic diagram of ASTM G98-17 galling test

3   Results

3.1   Microstructural characterisation

SEM

Top surface SEM images of the three coatings are presented in Figure 3. The EPHC coating exhibited a typical electroplated surface containing cracks and nodules; some features relating to the grinding marks of the underlying substrate were present but to a lesser degree than in the PVD coatings. The two PVD coatings exhibited visibly different top surface features. The EBPVD chromium appeared to have a characteristic PVD surface containing fine scale growth defects and parallel marks corresponding to the grinding features of the underlying substrate. The UMS PVD chromium coating exhibited similar features; however, it had a much coarser microstructure than the EBPVD as shown in the higher magnification images of the PVD coating top surfaces presented in Figure 4.
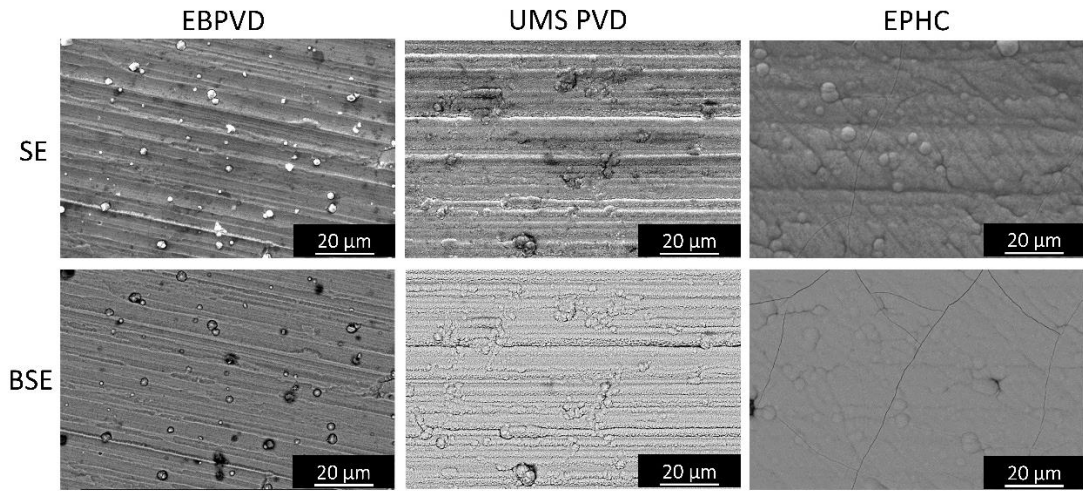
Figure 3 Top surface SE and BSE SEM micrographs of as-received EBPVD, UMS PVD and EPHC coatings
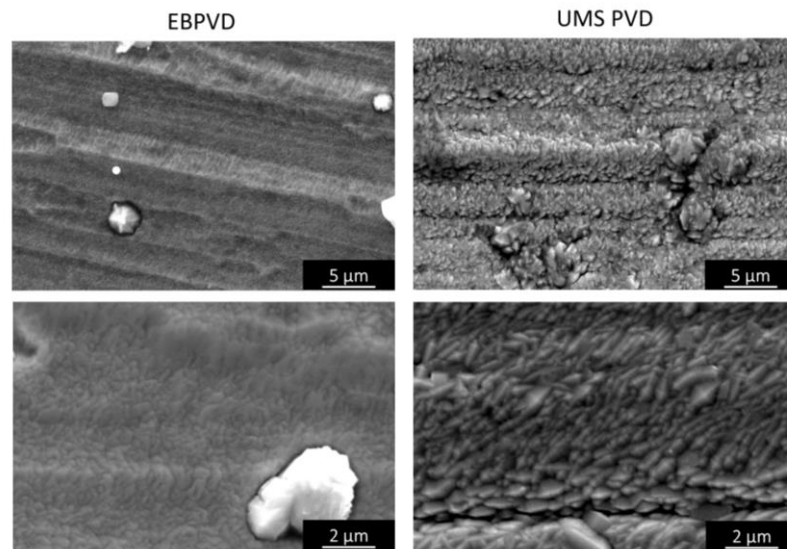

Figure 4 Top surface SE SEM micrographs of as-received EBPVD and UMS PVD coatings showing differences in coating structures

Elemental composition

EDX analysis of the top surfaces revealed little elemental difference on the coating top surfaces. All coatings were comprised of chromium. Impurities of tungsten (<0.3 at.%) were detected in the EBPVD coating and 1-2 wt% O_2 was also detected at the bright coating defects as seen in the SE SEM images (Figure 4). Impurity particles were not observed in the SEM on the top surface of the UMS coating.

Surface roughness

The EBPVD and UMS PVD coatings had similar surface roughness (Ra) values of 285 ± 8 nm and 351 ± 60 nm respectively. The electroplated Cr coating surface roughness was roughly twice that of the PVD coatings with an Ra of 613 ± 100 nm.

X-ray diffraction

X-ray diffraction (XRD) revealed that all coatings to were comprised of BCC chromium (ICDD-PDF-00-006-0694) (Figure 5). The EBPVD coating was observed to have a strong preferred orientation, with the {2 0 0} planes parallel to the coating surface, differing from the UMS PVD coating which had preferred orientations of the {1 1 0} and {2 1 1} planes parallel to the coating surface. The electroplated chromium revealed crystalline peaks which were relatively broad and of low relative intensity suggesting a fine grain size and/or internal microstrain in the grains. The EPHC coating presented a deviation in relative peak intensity in comparison with the powder diffraction crystallographic data entry.

The crystallite sizes of coatings were estimated using the (2 0 0) peak for all three coatings and corrected for instrumental broadening using a lanthanum hexaboride reference sample. The crystallite sizes estimated for the EBPVD, UMS PVD and EPHC were 42 nm, 108 nm and 25 nm respectively. However, it is recognised that the measured crystallite sizes are approximations and effects of microstrain are not accounted for when using the Scherrer equation.
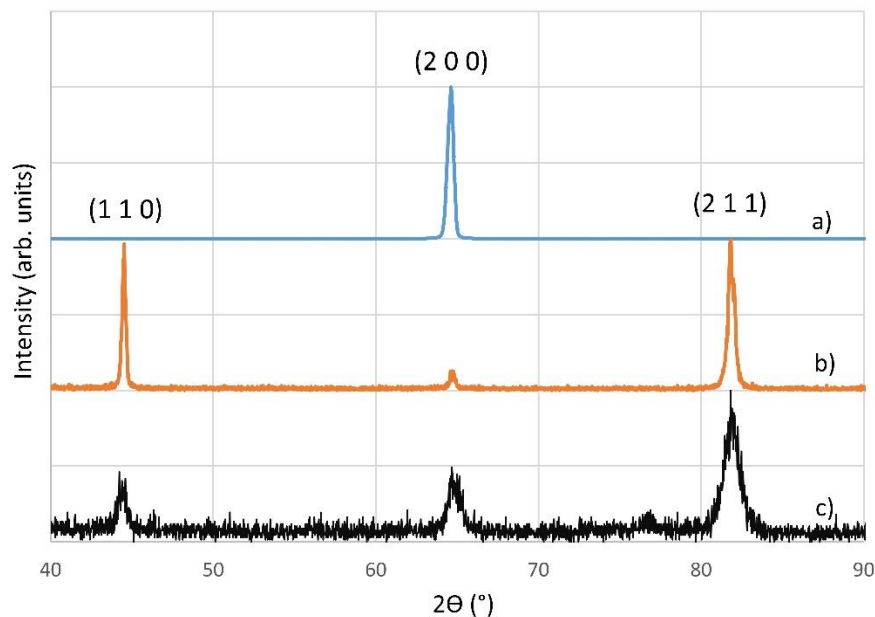

Figure 5 XRD patterns of top surfaces of chromium coatings normalised about the peak of maximum intensity showing differences in crystal orientation; (a) EBPVD (b) UMS PVD (c) EPHC

3.2   Mechanical testing

Hardness

Nanoindentation revealed the two PVD coatings to have similar hardness values of 5.0 ± 1.0 GPa for the EBPVD and 5.3 ± 1.3 GPa for the UMS PVD (Figure 6). The electroplated Cr, with a hardness of 10 ± 1.8 GPa, had approximately twice the hardness of the PVD coatings. The average maximum indentation depths for the EBPVD, UMS PVD and EPHC coatings were 920 ± 90 nm, 908 ± 97 nm and 685 ± 51 nm respectively.
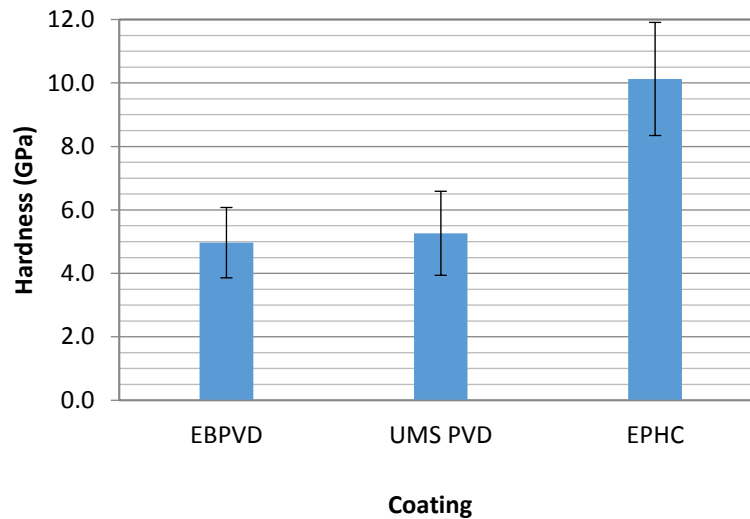

Figure 6 Mean hardness measured on the top surface of coatings showing a significant difference in hardness of the EPHC compared to the PVD coatings; error bars represent one standard deviation

Scratch testing

Due to the high thickness of the coatings, the scratch test is regarded as a test of the coatings fracture resistance rather than a test of the adhesion of the coatings as at the maximum load the test did not penetrate the entire thickness of the coatings. The EBPVD coating exhibited no signs of cracking up to the 90 N maximum load applied. The UMS PVD coating exhibited some signs of arc-type tensile cracking between 78 and 90 N load. The EPHC deposit exhibited multiple cracking at an average load of 16 N up to the maximum load of 90 N. Scratch scars on the coatings at the maximum load range of 78-90 N are presented in Figure 7.

Scratch scars (78-90 N)

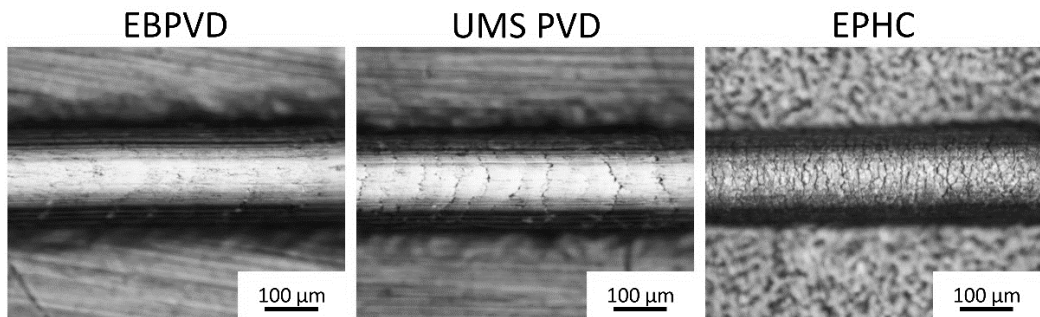| EBPVD	UMS PVD	EPHC

Figure 7 Optical microscopy images of scratch scars on the three coating types at the maximum load range of 78-90 N; some cracking was observed on the UMS PVD coating and significant cracking on the EPHC coating

Galling wear testing

As a reference, galling wear tests were conducted on uncoated self-mated 316 stainless steel. The uncoated pair showed signs of galling initiation at 7 MPa and increased damage at 15 MPa, as would be expected given the well-known poor galling resistance of this alloy.

Optical microscope images of the wear scars on the coated discs and 316 stainless steel counterfaces after galling testing are presented in Figure 8, with the galled areas being indicated on the coatings.

Galling tests on the EBPVD coating revealed that initial material transfer and coating delamination also occurred at a low stress of 7 MPa. Further damage occurred at 15 MPa as seen in Figure 8 (a & b). At higher loads of 22 MPa catastrophic failure of the coating was observed. The UMS PVD coating exhibited galling failure at a much higher load of 125 MPa (Figure 8 (c & d)). At lower loads, some scratching and small initiation sites of galling were observed but the coating remained mostly undamaged. The EPHC coating exhibited scratching, coating cracking, some signs of galling initiation and mild substrate deformation at 100 MPa. However, galling failure was not observed until a load of 125 MPa was reached (Figure 8 (e & f)).

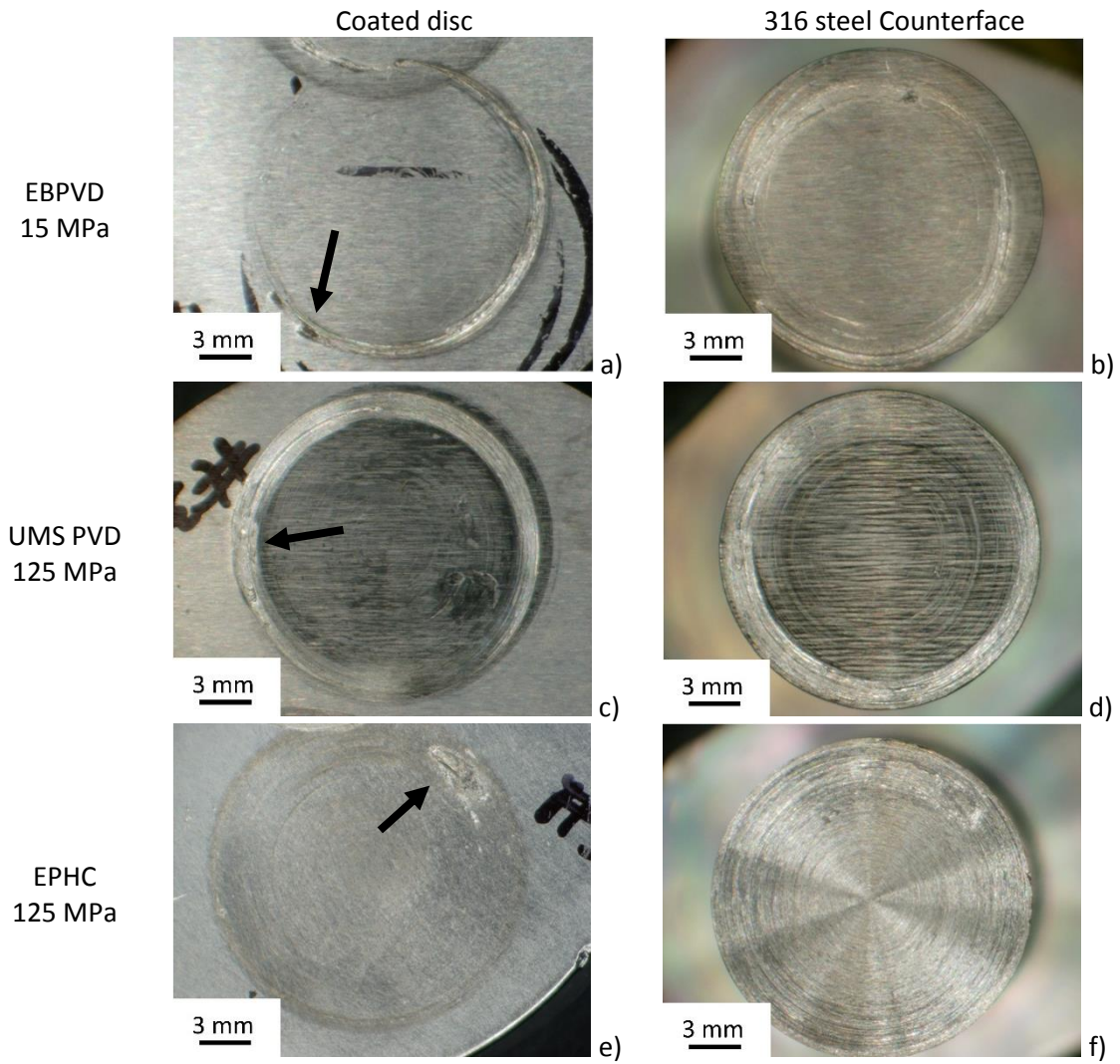|	Coated disc	316 steel Counterface
EBPVD 15 MPa	a)	b)
UMS PVD 125 MPa	c)	d)
EPHC 125 MPa	e)	f)

Figure 8 Optical microscopy images of wear scars on the coated discs and 316 stainless steel counterfaces after galling testing: (a & b) EBPVD coating at 15 MPa (c & d) UMS PVD coating at 125 MPa (e & f) EPHC coating at 125 MPa. Arrows indicate points of galling on coatings

SEM images of the top surface of the EBPVD coating after testing at 15 MPa reveal a clear difference in contrast in the BSE image along the wear scar indicating material transfer (Figure 9 (a)). Furthermore, EDX analysis confirmed the bright contrast material to be iron-rich suggesting either coating removal or transfer of steel from the counterface had occurred. The dark contrast (black) areas on the coating surface were confirmed to be oxygen rich. Cross sectional images taken chordally across the wear scar (~ parallel to direction of shear in the centre of the scar) reveal that the coating had either been removed or material had been transferred on top of the coating (Figure 9 (b)).
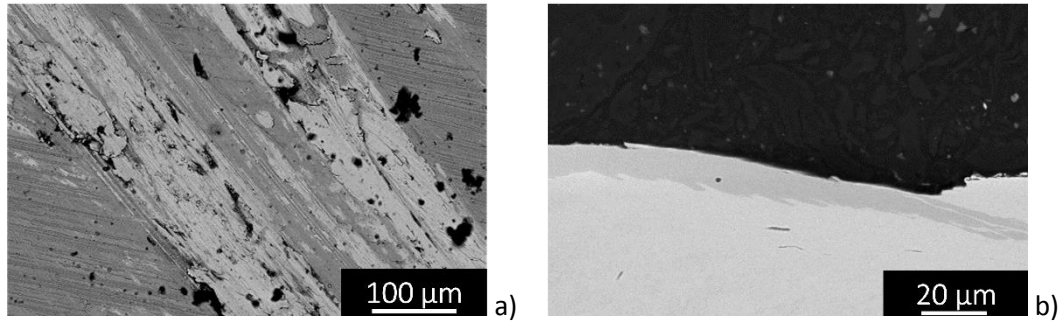
Figure 9 BSE SEM micrographs of wear scar on EBPVD coating after galling testing at 15 MPa: (a) top surface (b) chordal cross-section (~ parallel to direction of shear) where areas of coating removal are observed

SEM images of the top surface and cross-section of the UMS PVD tested at 125 MPa reveal a very different type of behaviour. There is clear evidence for coating delamination or material transfer and substantial plastic deformation at this high contact pressure (Figure 10). In some areas, the coating was still adhered to the substrate but plastic deformation of the coating had occurred as indicated by the directionality of defects highlighted in Figure 10 (b), noting that in an undeformed coating, these defects are generally perpendicular to the surface of the coating. Higher magnification SEM images of the coating top surface (Figure 10 (c)) reveal plastic deformation and flattening of the coating top surface.
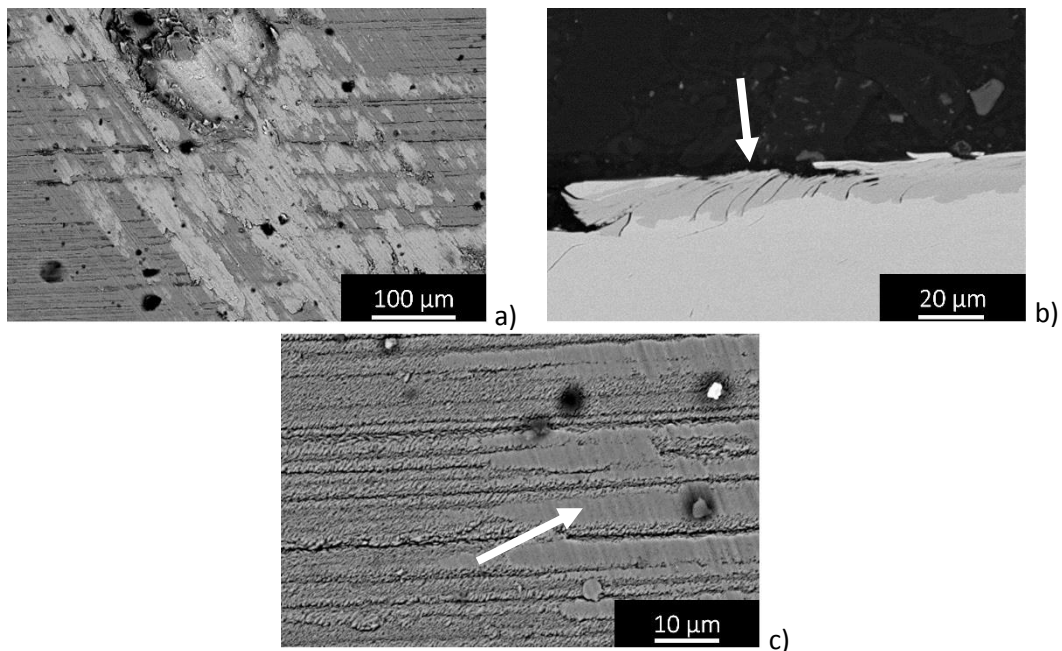

Figure 10 BSE SEM micrographs of wear scar on UMS PVD coating after galling testing at 125 MPa (a & c) top surface; (b) chordal cross-section (~ parallel to direction of shear) where plastic deformation is observed on the coating top surface as indicated by the arrow.

SEM images of the cross-section of the EPHC tested at 125 MPa reveal coating cracking and delamination as well as material transfer on top of the coating (Figure 11). Unlike the UMS PVD coating, little plastic deformation is observed and the main failure mechanism appears to be fracture and delamination.
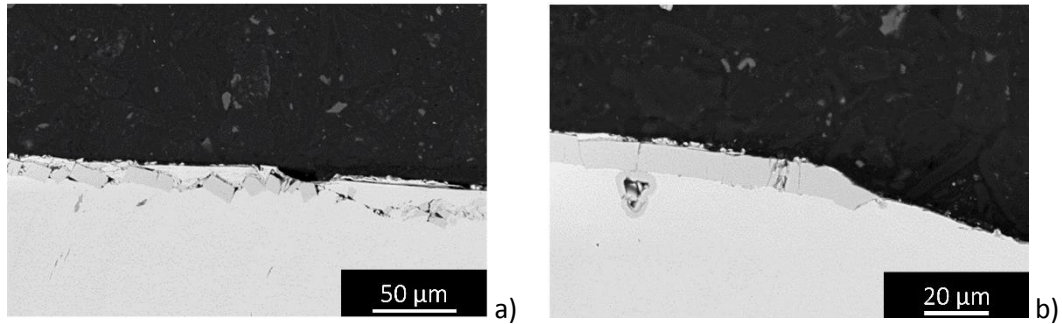
Figure 11 Chordal cross-sectional BSE SEM micrographs (~ parallel to direction of shear) of the EPHC coating after testing at 125 MPa; coating fracture, delamination and material transfer is observed

In order to elucidate further the mechanisms of failure, the cross sections of the wear scars were etched using Vilella's Reagent and the resultant microstructural features are shown in the OM images presented in Figure 12.
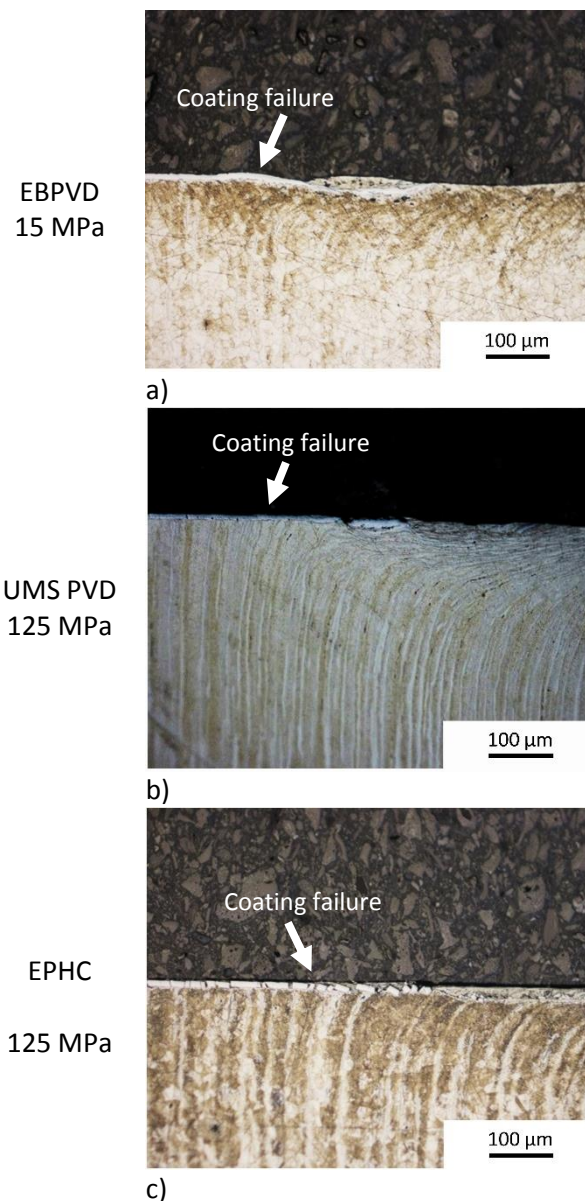

Figure 12 Optical microscopy of etched cross-sections of (a) EBPVD Cr coating after galling testing at 15 MPa (b) UMS PVD Cr after testing at 125 MPa (c) electroplated coating after testing at 125 MPa; substrate deformation is observed at the point of coating failure as indicated by the arrows

Clear substrate deformation is observed in areas of coating failure. For the EBPVD coating, substrate deformation was less severe due to the low contact stresses at which the coating failed. For the UMS PVD and EPHC coatings, the substrate deformation is seen to be severe in areas where the coating failed. However, little substrate deformation is observed in areas where the coating remained in place as seen by the lack of substrate deformation in the areas to the left of the point of coating failure in Figure 12. This suggests that severe substrate deformation only occurred at points where the coating had been removed and the substrate was in direct contact with the counterface; as such, the deformation of the substrate does not appear to be the determining factor of the coatings galling resistance.

4   Discussion

When studying the galling behaviour of coatings, it has been stated that the galling resistance of a coating can be improved by a thicker coating, higher hardness and lower surface roughness [19, 21]. In this work, the thickness, hardness and surface roughness of the two PVD coatings were similar (Figure 6). However, in galling testing, the UMS PVD coating failed at stresses between 5 and 10 times higher than that of the EBPVD coating (Figure 8). Galling tests revealed that the EBPVD provided no improvement in galling resistance compared to self-mated stainless steel.

It is argued that the EBPVD contained a higher density of surface defects compared to the UMS PVD, but, due to the structure of the UMS PVD coating, the defects were less visible (Figure 3 & Figure 4) and therefore, a direct comparison could not be made. The effect of PVD surface defects on the tribological properties of coatings has been investigated in previous studies which revealed that surface defects have a negative impact on the tribological properties of coatings as they can be a primary source of abrasive particles in sliding contact and high stresses can occur at these defects resulting in coating cracking. The reduction of these defects by polishing of the substrate and post-polishing of the coatings can improve coating performance. However, it is also revealed that post-polishing of coatings deposited on ground substrates resulted in little improvement as the presence of scratches on the surface originating from the underlying ground morphology dominates the wear behaviour. Coatings in this study were deposited onto ground substrates and therefore, it is expected that the presence of surface defects on the EBPVD coating was not the underlying factor for its low galling resistance [16].

When comparing the behaviour of systems, it is recognised that there will be many differences, some of which have been characterized in detail (such as the hardness) and others which have not (such as the residual stress). There is need to focus on the most significant differences, and for the two PVD coatings, their microstructure and crystal texture (Figure 4 & Figure 5) fall into this category. SEM images of the coating top surfaces revealed the UMS PVD coating to have a much coarser microstructure than the EBPVD (Figure 3 & Figure 4). The EBPVD coating had a strong preferred orientation in the {2 0 0} planes parallel to the coating surface whereas the UMS PVD coating had preferred orientations in the {1 1 0} and {2 1 1} planes parallel to the coating surface. It is known that BCC materials contain multiple slip systems, the dominating slip systems being {1 1 0}, {1 1 2} and {1 2 3} in the <1 1 1> direction and that plastic deformation occurs by dislocation motion along these planes [25-28]. In light of the above, it is a reasonable

hypothesis that the alignment of the {1 1 0} slip planes parallel to the surface results in the increased plastic deformation observed on the top surface and in the cross-section of the galled UMS PVD coating (Figure 10) compared to the EBPVD coating (Figure 9). Whilst it is proposed that this increase in plastic deformation benefits the galling resistance of the coating, this is currently not well understood and further research needs to be conducted to elucidate the damage mechanisms. Sriraman et al. [29] investigated the effect of crystal orientation on the tribological properties of Zn films. The study found that the crystal orientation did have an effect on the tribological properties, however, the films were also not of the same hardness and it was stated that it was this higher hardness (rather than the slip behaviour) that resulted in a higher wear resistance.

Although the EPHC was 1-2 μm thicker and almost twice the hardness of the UMS PVD coating, the sputtered coating performed similarly to the EPHC in galling tests. This can be attributed to the higher surface roughness of the electroplated coating or due to the inherent cracks in the coating which could have acted as initiation sites for galling. The high hardness of EPHC has been the subject of considerable speculation and study over many years, it has been attributed to multiple factors including the hydrogen and oxygen content in the films, small grain size and internal stresses [30]. In this coating, it is notable that galling damage is associated with fracture of the coating and rotation of sections of coating under the galling shear forces, rather than being associated with plastic deformation (Figure 11).

The results obtained in this study suggest that PVD chromium deposited by unbalanced magnetron sputtering has potential as a replacement for electroplated chromium in some tribological applications. However, the crystal orientation of the coating has been shown to play a significant role in its tribological behaviour, and thus the link between processing conditions and crystallographic texture needs to be further explored.

5   Conclusions

The two PVD Cr coatings examined in this work exhibit a high degree of crystallinity with clear preferred crystallographic orientations (texture); moreover, the nature of the texture depends on the deposition method. In contrast, EPHC coating exhibits a less perfect crystalline structure but with less significant texture.

The two PVD coatings exhibit similar indentation hardness values (~ 5 GPa) whereas that of EPHC has a hardness of ~ 10 GPa.

In the ASTM G98-17 galling test conducted against a grade 316 stainless steel counterface, EPHC and UMS PVD Cr coatings exhibited a similar galling resistance which is significantly higher than that of self-mated 316 steel. In contrast, the EBPVD Cr exhibits a similar galling resistance to that of self-mated 316.

It is suggested that the different deposition textures of EB and UMS PVD chromium play a key role in the galling behaviour and that hardness alone cannot be used as a predictor of galling resistance of coated components against 316 steel.

1. Liang, A., et al., *A favorable chromium coating electrodeposited from Cr(III) electrolyte reveals anti-wear performance similar to conventional hard chromium.* Materials Letters, 2017. **189**: p. 221-224.
2. Bikulčius, G., et al., *Dry sliding tribological behavior of Cr coatings electrodeposited in trivalent chromium sulphate baths.* Surface and Coatings Technology, 2017. **315**: p. 130-138.
3. Daure, J.L., et al., *The effect of coating architecture and defects on the corrosion behaviour of a PVD multilayer Inconel 625/Cr coating.* Surface and Coatings Technology, 2017. **324**: p. 403-412.
4. Liang, A., et al., *Structure characterization and tribological properties of thick chromium coating electrodeposited from a Cr(III) electrolyte.* Surface and Coatings Technology, 2013. **218**: p. 23-29.
5. Regulation (EC) No 1907/2006, *Concerning the Registration, Evaluation, Authorisation and Restriction of Chemicals (REACH), establishing a European Chemicals Agency, amending Directive 1999/45/EC and repealing Council Regulation (EEC) No 793/93 and Commission Regulation (EC) No 1488/94 as well as Council Directive 76/769/EEC and Commission Directives 91/155/EEC, 93/67/EEC, 93/105/EC and 2000/21/EC*. 2007. p. L136/3.
6. Mello, C.B., et al., *Corrosion effects of plasma immersion ion implantation-enhanced Cr deposition on SAE 1070 carbon steel.* Surface and Coatings Technology, 2011. **205**: p. S151-S156.
7. Navinšek, B., P. Panjan, and I. Milošev, *PVD coatings as an environmentally clean alternative to electroplating and electroless processes.* Surface and Coatings Technology, 1999. **116-119**: p. 476-487.
8. Paturaud, C., et al., *Correlation between hardness and embedded argon content of magnetron sputtered chromium films.* Thin Solid Films, 1999. **347**(1): p. 46-55.
9. Legg, K.O., et al., *The replacement of electroplating.* Surface and Coatings Technology, 1996. **81**(1): p. 99-105.
10. Wang, S.-F., et al., *Characterization of chromium thin films by sputter deposition.* Journal of Alloys and Compounds, 2011. **509**(41): p. 10110-10114.
11. Mello, C.B., et al., *Experimental study of mechanical and tribological behavior of nitrogen ion-implanted chromium thin films.* Surface and Coatings Technology, 2017. **312**: p. 123-127.
12. R, P., et al., *REVIEW OF PHYSICAL VAPOUR DEPOSITION (PVD) TECHNIQUES*. 2013.
13. Mattox, D.M., *Physical vapor deposition (PVD) processes.* Metal Finishing, 2001. **99, Supplement 1**: p. 409-423.
14. Li, B., et al., *Aluminum transfer buildup on PVD coated work rolls during thermomechanical processing.* Surface and Coatings Technology, 2016. **308**: p. 244-255.
15. Friedrich, C., et al., *PVD CrxN coatings for tribological application on piston rings.* Surface and Coatings Technology, 1997. **97**(1–3): p. 661-668.
16. Panjan, P., A. Drnovšek, and J. Kovač, *Tribological aspects related to the morphology of PVD hard coatings.* Surface and Coatings Technology, 2017.
17. Saketi, S. and M. Olsson, *Influence of CVD and PVD coating micro topography on the initial material transfer of 316L stainless steel in sliding contacts – A laboratory study.* Wear, 2017. **388-389**: p. 29-38.
18. Eriksson, J. and M. Olsson, *Tribological testing of commercial CrN, (Ti,Al)N and CrC/C PVD coatings — Evaluation of galling and wear characteristics against different high strength steels.* Surface and Coatings Technology, 2011. **205**(16): p. 4045-4051.
19. Karlsson, P., et al., *Galling resistance and wear mechanisms for cold-work tool steels in lubricated sliding against high strength stainless steel sheets.* Wear, 2012. **286-287**: p. 92-97.
20. Budinski, K.G. and S.T. Budinski, *Interpretation of galling tests.* Wear, 2015. **332-333**: p. 1185-1192.

21.   Klünsner, T., et al., *Influence of surface topography on early stages on steel galling of coated WC-Co hard metals.* International Journal of Refractory Metals and Hard Materials, 2016. **57**: p. 24-30.

22.   Voss, B.M., et al., *A new methodology for measuring galling wear severity in high strength steels.* Wear, 2017. **390-391**: p. 334-345.

23.   Patterson, A.L., *The Scherrer Formula for X-Ray Particle Size Determination.* Physical Review, 1939. **56**(10): p. 978-982.

24.   *ASTM Standard C1624-05, 2015, "Standard Test Method for Adhesion Strength and Mechanical Failure Modes of Ceramic Coatings by Quantitative Single Point Scratch Testing", ASTM International, West Conshohocken, PA, 2015, DOI: 10.1520/C1624-05R15, www.astm.org.*

25.   Naveen Kumar, N., et al., *Active slip systems in bcc iron during nanoindentation: A molecular dynamics study.* Computational Materials Science, 2013. **77**: p. 260-263.

26.   Serenelli, M.J., M.A. Bertinetti, and J.W. Signorelli, *Investigation of the dislocation slip assumption on formability of BCC sheet metals.* International Journal of Mechanical Sciences, 2010. **52**(12): p. 1723-1734.

27.   Weinberger, C., B. Boyce, and C.C. Battaile, *Slip planes in bcc transition metals*. Vol. 58. 2013. 296-314.

28.   Verma, R.K., et al., *Modelling anisotropic hardening of an ultra low carbon high strength steel using crystal plasticity.* Materials Science and Engineering: A, 2013. **559**: p. 359-363.

29.   Sriraman, K.R., et al., *Effect of crystallographic orientation on the tribological behavior of electrodeposited Zn coatings.* RSC Advances, 2016. **6**(21): p. 17360-17372.

30.   Brenner. J, B.P., Jennings. C, *Physical Properties of Electrodeposited Chromium.* Journal of Research of the National Bureau of Standards 1948. **40**: p. 31-59.